CORA Cork Open Research Archive
Cartlann Taighde Oscailte Chorcaí

Title	Key enabling technologies for optical communications at 2000 nm
Authors	Gunning, Fatima C. Garcia;Kavanagh, Niamh;Russell, Eoin;Sheehan, Robert;O'Callaghan, James;Corbett, Brian M.
Publication date	2018-06-25
Original Citation	Gunning, F. C. G., Kavanagh, N., Russell, E., Sheehan, R., O'Callaghan, J. and Corbett, B. (2018) 'Key enabling technologies for optical communications at 2000 nm', Applied Optics, 57(22), pp. 64-70. doi:10.1364/AO.57.000E64
Type of publication	Article (peer-reviewed)
Link to publisher's version	10.1364/AO.57.000E64
Rights	© 2018, Optical Society of America. Provided under the terms of the OSA Open Access Publishing Agreement. Users may use, reuse, and build upon the article, or use the article for text or data mining, so long as such uses are for non-commercial purposes and appropriate attribution is maintained. All other rights are reserved.
Download date	2023-05-05 01:34:43
Item downloaded from	http://hdl.handle.net/10468/6751

UCC
University College Cork, Ireland
Coláiste na hOllscoile Corcaigh

applied optics

Key enabling technologies for optical communications at 2000 nm

F. C. Garcia Gunning,* N. Kavanagh, E. Russell, R. Sheehan, J. O'Callaghan, and B. Corbett

Tyndall National Institute and Department of Physics, University College Cork, Lee Maltings, Dyke Parade, Cork T12 R5CP, Ireland
**Corresponding author: fatima.gunning@tyndall.ie*

Received 9 April 2018; revised 28 May 2018; accepted 29 May 2018; posted 30 May 2018 (Doc. ID 327995); published 25 June 2018

This paper discusses the potential for opening a new wavelength window at the 2 μm waveband for optical communications, showing current limitations of the system's performance. It focuses on novel results for key enabling technologies, including the analysis of laser injection locking at this waveband, an improved responsivity for bulk and strained InGaAs edge-couple detectors, and also an increased gain profile for thulium-doped fiber amplifiers. © 2018 Optical Society of America

OCIS codes: (060.4510) Optical communications; (060.2390) Fiber optics, infrared; (060.2340) Fiber optics components; (230.4480) Optical amplifiers; (250.0040) Detectors.

https://doi.org/10.1364/AO.57.000E64 Provided under the terms of the OSA Open Access Publishing Agreement

1. INTRODUCTION

The emerging bandwidth (BW) hungry applications, such as autonomous vehicles, augmented reality for industrial applications, as well as the gaming and film industry, in addition to high-definition video, such as 4k, 8k, and beyond, require high-capacity optical communications with low latency. The infrastructure is currently enabled by dense wavelength division multiplexing (DWDM), originally at 10 Gbit/s per channel, but swiftly upgrading to 100 Gbit/s per wavelength with commodity coherent detection available in the market. In fact, the standardization of coherent detection is allowing for further network improvements with a movement towards 200, 400, and even 600 Gbit/s per channel, enabled by higher-order modulation formats [e.g., 64 quadrature amplitude modulation (QAM)], dual polarization, and digital signal processing (DSP) at both transmitters and receivers [1]. Traditional impairments, such as loss, dispersion, and nonlinearities, are still present with losses being mitigated by erbium-doped fiber amplifiers (EDFAs) and dispersion by DSP with novel algorithms to mitigate, at least in part, nonlinearities. Although we can foresee all of these technologies implemented on the ground for the next 10 years, radical options must be sought for the future. Emerging alternatives rely on novel optical fibers; either via spatial division multiplexing (SDM) to expand capacities at 1550 nm [2], but requiring significant DSP, or exploring fibers that minimize impairments, such as hollow-core photonic bandgap fibers (HC-PBGF) or antiresonant hollow-core fibers, which aim to reduce nonlinearities while improving latency [3]. HC-PBGF, for example, was shown to propagate light at ~98% of c [4] with a potential minimal loss of ~0.2 dB/km around 2000 nm [5]. The extended nonlinear threshold could enable capacities beyond current single-mode fiber (SMF) limits, for example, with potential applications in short haul communications requiring high optical signal to noise ratio (OSNR) and/or low latency [6].

Back in the 1980s, before the EDFA's revolution, researchers were investigating novel optical fiber materials, such as ZrF_4 – BaF_2 – LaF_3 – AlF_3 – NaF (ZBLAN), fluoride, and chalcogenite, to reduce the intrinsic loss, moving away from Rayleigh scattering, further into the infrared, and below infrared absorptions [7]. The first, to the best of our knowledge, transmission experiments using semiconductor lasers at 2400 nm dates back to 1987 with 34 Mbit/s single-channel transmission [8]. Such fibers, however, were brittle and highly nonlinear, which prevented propagation over longer distances. Today, however, HC-PBGF is presented as a real alternative. With optical fiber drawing processes improving and with longer lengths possible, exploring a new wavelength window around 2000 nm now arises with the benefit of high-quality lasers operating at this waveband [9]. This is also an attractive waveband for silicon photonics, enabling efficient nonlinear processes with diminished undesirable two-photon absorption effects [10]. For example, in the last couple of years, a wealth of novel silicon-based or silicon-integrated devices operating at this waveband have been demonstrated, such as photodiodes [11,12], arrayed waveguide gratings (AWG) [13], semiconductor optical amplifiers [14], and demultiplexers handling 1.55 and 2 μm signals, to name a few [15].

We have shown previously that the first generation devices were capable of delivering DWDM with 100 GHz spaced channels and a total capacity of 100 Gbit/s [16]. Capacities reaching 30 Gbit/s were achieved with the aid of advanced

modulation formats that still use direct detection [17]. But, the technologies are far from optimal. For example, heterodyne coherent detection at this waveband was shown for sensing applications at low bit-rates [18], but polarization diverse coherent detection at high speeds continues to be researched with recent advances in designing hybrids [19] and the first, to the best of our knowledge, balanced detector chips just fabricated at Tyndall. Novel TiO_2 [20] and SiGe waveguides [21] have also shown 10 Gbit/s performance at 2 μm. In this paper, we show in Section 2, as an example, that increasing the spectral efficiency further by reducing the channel spacing to 50 GHz requires novel filtering technologies, as narrow filters are not available at this waveband, although potential exists with silicon photonics [22]. We discuss the potential for injection locking and show a detailed performance of stable injection locking at 2000 nm.

In addition, we will focus on the recent developments of another two key enabling technologies to further explore the new wavelength window at 2000 nm. We discuss the potential for InGaAs edge-coupled detectors in contrast with surface-emitting detectors in Section 3 and also the optimization avenues for thulium-doped fiber amplifiers (TDFA) in Section 4. TDFAs have a critical role, just as EDFAs did for the C band, in providing gain for compensation fibers and component losses. As a rule of thumb, assuming a rough estimate of the predicted loss of HC-PBGF to be similar to a SMF at 0.2 dB/km, TDFAs with gains between 20 and 25 dB would be required, enabling over 80km transmission under the same OSNR.

2. SYSTEM PERFORMANCE

A. Limitations of a 50 GHz Spacing DWDM at 2000 nm

Figure 1 is an example of a back-to-back experimental setup for DWDM at 2000 nm with the major components used for this experiment described in detail in Ref. [23]. The lasers used were highly strained $In_{0.75}Ga_{0.25}As$ multiple quantum-well ridge-waveguide laser structures grown on InP substrates and designed for single-mode operation [9]. Polarization controllers (PCs) were added to ensure co-polarized signals prior to data-encoding. Two additional directly modulated channels are depicted here (channel #6 and channel #8, labelled as the "even" channels) to emulate a scenario with a narrow 50 GHz spacing around the channel under test, also known as channel #7.

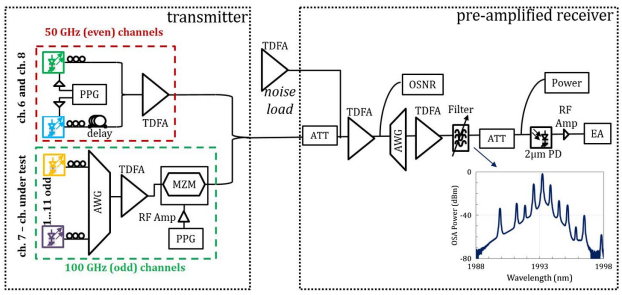

Fig. 1. DWDM experimental setup for 100 and 50 GHz channel spacing. Left, transmitter configurations; right, receiver. Inset shows the received spectrum of channel #7, the channel under test when 50 GHz emulation is on.

These two lasers were directly modulated with non-return-to-zero on–off keying (NRZ-OOK) at a data rate of 8 Gbit/s with a pseudo-random sequence of $2^{31} - 1$ from a pulse pattern generator (PPG). This scheme enables a simultaneous comparison between our previously reported result at 100 GHz spacing [16] and emulating a 50 GHz spacing scenario. The bias and drive signals of both lasers were optimized in order to investigate the impact of the 50 GHz contribution. The reduced bit-rate was due to the limited frequency response of the lasers, as in Ref. [24]. The two "even" channels were then amplified using a commercial TDFA (AdValue Photonics 2 μm fiber amplifier).

For the 100 GHz spacing channels, six ("odd") channels were externally modulated with NRZ-OOK via a 9.5 V_π commercially available $LiNbO_3$-based Mach–Zehnder modulator (MZM, Photline MX200-LN-10), driven by a pseudo-random binary sequence (PRBS) length of $2^{31} - 1$ at a data rate of 12.5 Gbit/s from a second independent PPG and an RF amplifier. The 100 GHz signals were combined using an InP-based AWG, which was thermally tuned to match the required wavelengths and fixed at 25.6°C with an average insertion loss of ∼18 dB. To compensate for this loss, the output signal was amplified using another TDFA. The 100 GHz "odd" channels were multiplexed with the two "even" channels using a simple 2:1 fiber coupler.

The receiver is also described in Ref. [23]. Selecting each DWDM channel at the receiver is not trivial at 2000 nm, as currently available tunable bandpass filters have a 3 dB BW of ∼1.6 nm (Agiltron Inc. FOTF 043121333), and the in-house AWG used here hasve a side-mode suppression ratio of ∼18 dB [16]. Thus, by cascading both devices, channel isolation improves (for 100 GHz spacing) to ∼26 dB [23]. A noise-load system was added to vary the OSNR in conjunction with the receiver attenuator in order to ensure sufficient power reaches the detector. An extra TDFA was added to compensate for the AWG losses, and a second attenuator ensured a constant power of −2.2 dBm at the detector. Although a 26 dB channel isolation was measured for DWDM channels at 100 GHz spacing, when emulating a 50 GHz case, the isolation ratio deteriorates. The inset in Fig. 1 shows the filtered signal at the receiver with the channel isolation reducing to ∼10 dB, which is not sufficient for accurate bit error rate (BER) analysis.

Measurements showed that the average OSNR required to achieve a BER of 1×10^{-6} was found to be ∼27 dB [23] with minimal variation between the 100 or 50 GHz cases. This significantly differs from expectations of a much larger OSNR requirement for the worst case (all channels on). We believe this could be attributed to the limited extinction ratio of the filtering in the receiver, contributing randomly to the BER of the channel under test. This result, although not expected, calls for alternative methods for filtering in the receiver.

B. Injection Locking at 2000 nm—A Path to Filtering

In Section 2.A, we investigated the impact of decreasing the spacing of DWDM channels in the 2000 nm waveband from 100 to 50 GHz. While 50 GHz spacing can be readily achieved in the transmitter, there are several challenges in terms of the receiver, the most critical of which are available filtering techniques to accurately analyze the performance of the channel

under test. At 1550 nm, injection locking was shown to improve filtering [25] for data recovery [26] and to increase BW [27]. At 2000 nm, injection locking was shown to narrow the linewidth of lasers to permit higher-order modulation formats [17].

The phenomenon of injection locking occurs when light from a master laser (λm) is injected into the cavity of a slave laser (λs). If the fields of the master and the slave lasers are sufficiently close, the master can force the slave to oscillate at the same frequency as (and at a fixed phase relative to) the master laser. This $\lambda m = \lambda s$ behavior is observable for a certain range of master wavelengths close to the main lasing mode of the slave laser λs, called the locking range. Within this locking range, if λm is changed, λs will follow it accordingly. Finally, when the detuning ($|\lambda m - \lambda s|$) exceeds a certain value, the lasers will unlock (at this point $\lambda s \neq \lambda m$), and the slave no longer follows the master [28].

We demonstrated previous injection locking at 2000 nm by varying the temperature of the master laser [29]. Here, we show for the first time, to the best of our knowledge, the case when the slave laser is tuned to lock to the master. In other words, injection locking is achieved by varying the slave laser temperature (and therefore wavelength), while holding the master wavelength constant. This would emulate the case from Section 2.A, where the receiver must "tune" to the incoming DWDM channel. The experimental setup is depicted in Fig. 2 and is typical for injection locking schemes. The components used were previously described in Ref. [29], but, in detail, the master laser is coupled to a circulator port P1, which then launches the signal to P2, the slave laser. PCs are added in order to ensure injection and locking. The slave laser used here had only one integrated isolator of ~20 dB, enabling injection. The output of the slave was then sent back to the circulator to port P3, where the signal was amplified by a TDFA. The coupled output at P3 of the master and the slave lasers and the effect of injection locking therein were analyzed using an optical spectrum analyzer (OSA) and an electrical spectrum analyzer (ESA).

In the electrical domain, the use of a square-law detector (PD) enables a beat-note to be measured at a frequency corresponding to the detuning ($|\lambda m - \lambda s|$). As the detuning is reduced, the frequency of this beat-note decreases until the point at which the laser fields are sufficiently close so that injection locking occurs ($\lambda s = \lambda m$) and, in this case, no peak should be observed on the ESA. Due to the limited operating BW range of the 2000 nm PD used (EOT ET-5000F InGaAs PiN detector) with the ESA (3 dB BW of 12.5 GHz), the frequency detuning between λs and λm should be no greater than 20 GHz, which corresponds to ~0.27 at 2000 nm.

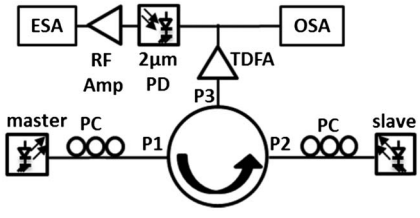

Fig. 2. Injection locking experimental setup.

For this reason, locking the slave to the master's main lasing mode was investigated, rather than locking to a side-mode. In the absence of a high-resolution tuneable laser source around 2000 nm, it was necessary to tune the operating wavelength of the lasers by adjusting the temperature. In this way, the wavelength of the slave laser (λs) was adjusted by varying the temperature ($\Delta\lambda s/\Delta T$ was measured to be 0.11 nm/°C), while the master temperature (Tm) was constant throughout. Both lasers were temperature controlled by a quad-laser driver (ILX LDC 3900), which allows control of four lasers simultaneously, but independently. The temperature stability was assumed to be the same as that of the driver or $< \pm 0.01$°C, as per specifications.

The resulting spectra of the coupled output from P3 are shown in Fig. 3, with the electrical spectra shown on the left and the corresponding optical spectra to the right, for decreasing Ts from 13.2°C to 12.4°C in steps of 0.1°C, with results presented here in steps of 0.4°C in order to demonstrate the slave at the edge of the locking region, locked and just outside the locking range. In Fig. 3(a), a beat-note is recorded at ~3 GHz. At 13.2°C, the slave is just at the edge of the locking region, and in Fig. 3(b)—the corresponding optical spectrum —the optical peaks are indistinguishable due to the resolution of the OSA (0.05 nm or 3.75 GHz). Figure 3(c) shows injection locking at $Ts = 12.8$°C; no beat-note is recorded inside the locking region, and, in Fig. 3(d), single-wavelength emission is observed ($\lambda s = \lambda m$). In Fig. 3(e), at $Ts = 12.4$°C, the slave has moved out of the locking region, and a beat-note

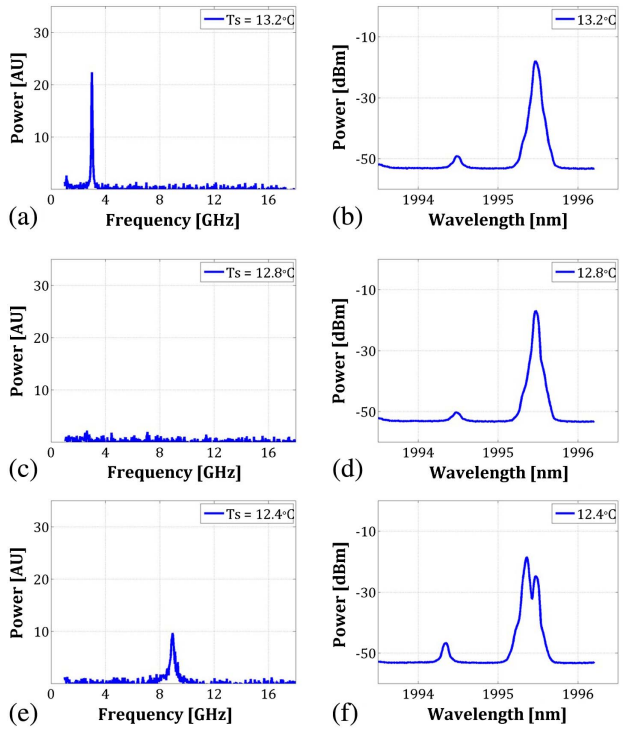

Fig. 3. Spectra of coupled master and slave lasers. Electrical spectra shown on the left and corresponding optical spectra to the right for decreasing Ts from 13.2°C to 12.4°C in steps of 0.4°C. Injection locking to λs is observed at $Ts = 12.8$°C. During the locking range, $\lambda s = \lambda m$ in the optical domain, and no peaks are measured in the electrical domain.

reappears at 9 GHz. This beat-note is relatively weak due to the limited operating range of the PD. With the lasers unlocked, both optical peaks are observed in Fig. 3(f).

We have demonstrated injection locking between two single-mode semiconductor lasers at 2000 nm; this was observed both optically and electrically. As the stability of the injection locking was only dependent on the stability of the temperature controller, applications both in the transmitter and in the receiver are likely. In the transmitter side, we aim to use injection locking for advanced system schemes, such as reducing linewidth to enable advanced modulation formats, while at the receiver, we expect to use this key enabling technology to enhance filtering for DWDM applications.

3. PHOTODETECTORS

Detectors based on strained InGaAs on InP substrates have demonstrated high-speed operations in the 2000 nm wavelength band. Table 1 shows a brief comparison of the responsivity and BW for absorber regions consisting of thick strain-relaxed InGaAs and thin, strained, but unrelaxed, multi-quantum-well (MQW) structures in surface and edge illuminated arrangements. Edge illuminated devices are preferable for fiber-coupling using lensed or butt-coupling configurations. Edge-coupling also separates the absorbing direction from the carrier collection direction, and, although large 3 dB $-$ S_{21} responses [3 dB BW) were measured previously, limited responsivities were achieved with MQW devices due to the low number of quantum wells employed. In this work, we show that a thicker bulk absorber enhances the responsivity of edge-coupled devices while maintaining a BW of ~6 GHz.

A 2000 nm thick strain-relaxed $In_{0.7}Ga_{0.3}As$ absorber was clad by a wider bandgap ($\lambda_g = 1840$ nm) *p*- and *n*- type $In_{0.7}(Al_{0.2}Ga_{0.8})_{0.3}$ to form a transverse waveguide. Lateral ridge waveguides of widths from 4–6 μm were etched through the absorbing structure, and detectors were fabricated with high-speed electrodes in a ground–signal–ground (GSG) configuration. A picture of the device is shown in Fig. 4. Previous results using this material as photodetector in the surface normal configuration (diameters 30–60 μm) have shown that it can be used to successfully to detect high-speed data signals transmitted at 2000 nm wavelengths [31].

The basic properties of the photodetector, such as current–voltage (IV) characteristics, dark current, and responsivity, were measured with the device set at a temperature of 25°C. The IV curve shows that the diode has an electrical ideality of 1.7, which is close to the previously reported value of 1.5 for this material [32]. The dark current for the device was measured to

Table 1. InGaAs Detector Comparison Operating at 2 μm

Device Type	Coupling	R (A/W)	3 dB BW (GHz)	Ref.
InGaAs MQWs	Edge	0.3	10	[30]
InGaAs MQWs	Edge	0.3	10	[31]
InGaAs Bulk	Surface	0.94	6	[31]
InGaAs Bulk	Surface	0.93	10	[32]
InGaAs Bulk	Edge	0.73	6	this work

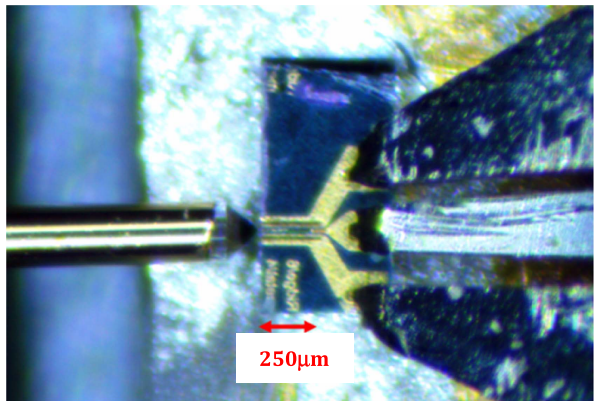

Fig. 4. Photograph of edge-coupled photodetector under test. Lensed fiber (left) illuminates the absorbing region of the photodetector. Incoming signal is detected electrically using GSG RF probe. Length of the PD under test is approximately 250 μm.

be –0.9 μA when the photodetector was reverse biased at –2 V and is reduced when compared to the surface normal devices. The photodetector responsivity was measured by coupling light from a single-mode laser emitting at a 2005 nm wavelength into the absorbing region of the photodetector using a lens-ended optical fiber. The output power of the laser was varied in order to characterize the photocurrent against it. Figure 5 shows a sample of the measured photocurrent versus bias voltage when the laser power varied from 0.78 to 2.44 mW. The responsivity was estimated to be 0.73(±0.03)A/W, which is approximately half the responsivity estimated for the surface normal device reported in Ref. [32] (or 1.3 A/W).

The reduced responsivity is due to the reduced coupling efficiency in the waveguided configuration and the lack of an antireflection coating on the input facet. Nevertheless, the value estimated for the edge-coupled device characterized here is more than twice the responsivity of an InGaAs MQW structure reported in Ref. [31] (or 0.3 A/W).

Further analysis of the RF small signal BW of the edge-coupled photodetector was carried out to estimate the 3 dB BW. A lens-ended optical fiber was used to couple the modulated light at a wavelength of 2005 nm into the photodetector. An external $LiNbO_3$ MZM (Photline MX200-LN-10) was used to convert the electrical signal from the vector network

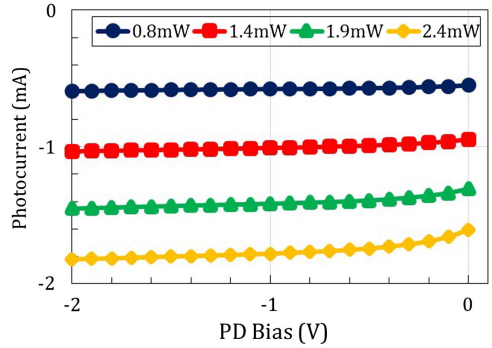

Fig. 5. Measured photocurrent against PD bias for varying input optical power (legend). The device temperature was maintained at 25°C.

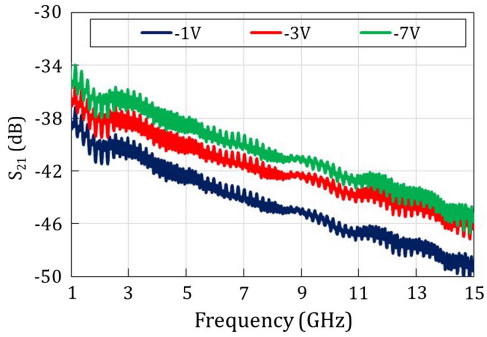

Fig. 6. Frequency response of the edge-coupled photodetector for different biases (legend), data indicates that the 3 dB bandwidth of the detector is approximately 6 GHz.

analyzer (VNA) into the optical domain and, hence, to analyze the S_{21} parameter of the photodetector. The S_{21} curves are displayed in Fig. 6 and show that the device has a 3 dB BW of ~6 GHz. The periodic fluctuations observed are either due to electrical reflections between the photodetector and the electrical RF cable to the VNA or, most likely, due to a short resonant cavity formed between the fiber and the detector, which was also caused by the lack of an antireflective coating on the input facet. As per Table 1, the measured 3 dB BW is similar as that reported for surface normal devices made from the same material reported in Ref. [31]. These are encouraging results, showing the potential of the device developed here.

4. THULIUM-DOPED FIBER AMPLIFIERS

Finally, another important key enabling technology to achieve communications at ~2000 nm is the availability of TDFAs in order to compensate for optical fiber and component losses. Current systems demonstrations at this waveband, in fact, show that TDFAs are used mostly to compensate for the non-ideal devices, and, hence, broad gains with low noise figures are required. TDFAs were also shown to amplify a broad range of optical signals, varying between 1700 and 2100 nm [33], but they can also be used as broadband sources based on their wide optical output generated by amplified spontaneous emission (ASE). For example, TDFAs were shown to facilitate CO_2 [34] and HCl sensing, the first peaking at ~2000 nm, while the second peaked at ~1742 nm.

The principle of operation is rather simple, resembling EDFAs. TDFAs consist of a strand of thulium-doped silica optical fiber (OFS TmDF 200), which is optically excited using a pump laser of higher energy, creating a gain medium that amplifies signals of wavelengths within the emission spectrum of thulium. Here, we show that an optimum TDFA configuration for broad ASE emission is based on a dual-pumping scheme. Here, a pump laser operates at 1550 nm (Princeton Lightwave) and the other at 785 nm (ThorLabs FPL785-250) with different absorption and emission mechanisms. For longer lengths of TDFs, a 1550 nm pump provides a better gain due to a well-distributed optical power density along the fiber length. This high-power distribution is caused by the low absorption coefficient of thulium at 1550 nm. This low

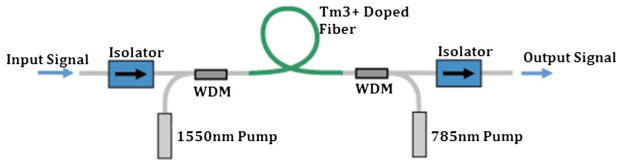

Fig. 7. Experimental setup for a dual-pumped TDFA.

absorption coefficient means 1550 nm of light is absorbed over the whole length of the fiber, leaving very little thulium unexcited through the length. For shorter lengths of fiber, a 785 nm pump produces better gain due to thulium's high absorption coefficient at 785 nm [35]. This high absorption means light at 785 nm is absorbed over a short length of the thulium-doped fiber (TDF), approximately 0.5 m. If pumped by 785 nm alone, the remainder of the fiber is left unexcited and reabsorbs the just amplified signals, reducing the effectiveness of longer TDFAs pumped at 785 nm. Hence, here, we show that a dual-pumping scheme with two simultaneous pumps can be used to optimize the TDFA's performance for both very short (0.5 m) and longer (2 m) lengths of TDFs.

Figure 7 shows the TDFA design used in this experiment. The dual-pump scheme exploits the absorption mechanisms described above with a 1550 nm laser forward pumping and a 785 nm laser reverse pumping (or backward pumping) the TDF. Wavelength specific WDM couplers were used to optimize the coupling of the signal and pump lasers and minimize the optical loss. Isolators were used to prevent ASE returning to the signal lasers and reducing their efficiency or even damaging them. Here, we chose relatively low power pump lasers, when compared to the literature, with the 1550 nm pump laser operating at 150 mW, and the 785 nm laser operating at 250 mW. All signal lasers were operating in the small signal regime (P_{signal} ~ −20 dBm). The length of TDF was varied in order to analyze the emission BW and also the gain dependence.

The ASE output of the TDFA was recorded for 0.5, 1, 1.5, and 2 m of TDFs. It can be seen in Fig. 8 that the spectrum shifts towards longer wavelengths as the length of fiber increases. This is caused by re-absorption of short wavelengths with fiber length. The number of unexcited thulium ions in the fiber increases for a given pump power. These unexcited ions absorb shorter wavelengths propagating through the fiber and re-emit at longer wavelengths. This causes the spectral shift

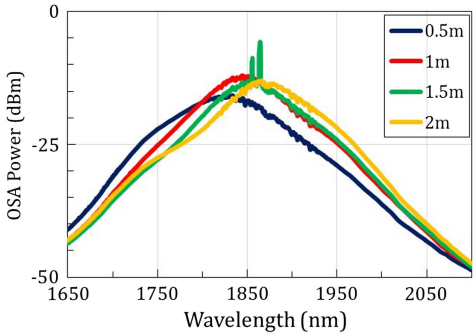

Fig. 8. ASE spectra for varying lengths of TDF.

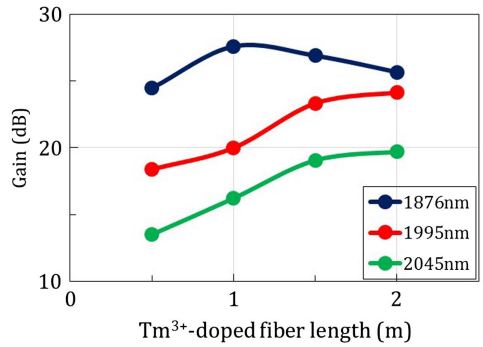

Fig. 9. Gain versus TDF length for varying signal wavelengths.

seen in Fig. 8. As the absorption spectrum of thulium ranges from 1500 to 1750 nm, it is expected that for lengths beyond 2 m the gain spectrum will continue to shift to longer wavelengths until emitted photons of wavelengths up to 1750 nm are fully re-absorbed. However, this will narrow the emission spectrum, which may not be desirable for some applications.

Figure 9 shows how the shift in ASE output translates into achievable optical gain for different wavelengths in the spectrum. For an 1876 nm signal, the maximum gain of 27 dB is achieved at 1 m. After this point, the gain begins to decline as the amplification spectrum shifts towards longer wavelengths. This shift in the amplification spectrum increases the gain for both the 1995 and 2045 nm signal to 24 and 18 dB, respectively. This shift in the amplification spectrum can be reduced by increasing the pump power exciting the TDFA, as this would reduce the number of unexcited thulium ions available to re-absorb the shorter wavelengths. However, higher-power pumps are costly, and it is perhaps unnecessary to increase the pump power if amplification is only required for specific wavelengths. In this case, the TDF's length can be adjusted to optimize the gain for a particular application or wavelength range. For example, HC-PBGF is predicted to have a low loss transmission between 1900 and 2100 nm [36]. For this fiber, it is unnecessary to have amplification at the lower wavelengths, and, hence, by increasing the TDF's length, higher pump powers are not required.

The effect of the TDF'S length on wavelength specific gain was characterized. An increase in gain is observed for all three wavelengths measured when moving from 0.5 to 1 m in the TDF's lengths. However, increasing the length further reduced the gain for the short wavelength laser (1876 nm), but no apparent reduction is observed for the other two sources at 1995 and 2045 nm. The maximum gains achieved were 27 dB at 1876 nm, 24 dB at 1995 nm, and 19 dB at 2045 nm with remarkably low pump powers when compared to the literature.

5. FINAL REMARKS AND CONCLUSIONS

We have shown here that there are several emerging technologies to enable optical communications at 2000 nm. Challenges are still many, and improvements are still required, in particular, to enable ultra-high capacities. Remarkably, pushing the band-edge further in the infrared was very successful by straining the InGaAs lattice, and the devices have shown reliable and stable performance.

Undoubtedly, the components and techniques here developed for wavelengths around 2000 nm are, not only, some of the key enabling technologies to open a new wavelength window, but they also enable such devices to be used in different research fields, such as gas sensing and biomedical applications.

Funding. Science Foundation Ireland (SFI) (12/RC/2276, 13/CDA/2103); Irish Research Council (GOIPG/2014/637, GOIPG/2017/385); FP7 Information and Communication Technologies (ICT) (258033).

Acknowledgment. The authors acknowledge the support and discussions from Eblana Photonics and the Optoelectronic Research Centre (ORC), and David Goulding (CIT) and Padraic Morrissey (Tyndall).

REFERENCES

1. X. Zhou and L. Nelson, "Advanced DSP for 400 Gb/s and beyond optical networks," J. Lightwave Technol. **32**, 2716–2725 (2014).
2. A. V. Turukhin, O. V. Sinkin, H. G. Batshon, M. Mazurczyk, M. A. Bolshtyansky, D. G. Foursa, and A. N. Pilipetskii, "High-capacity SDM transmission over transoceanic distances (invited)," in *Optical Fiber Communications Conference and Exhibition (OFC)* (2018), paper W1B.6.
3. D. J. Richardson, N. V. Wheeler, Y. Chen, J. R. Hayes, S. R. Sandoghchi, G. T. Jasion, T. D. Bradley, E. N. Fokoua, Z. Liu, R. Slavik, P. E. Horak, M. N. Petrovich, and F. Poletti, "Hollow core fibers and their applications," in *Optical Fiber Communications Conference and Exhibition (OFC)* (2017), paper Tu3H.1.
4. F. Poletti, N. V. Wheeler, M. N. Petrovich, N. Baddela, E. Numkam Fokoua, J. R. Hayes, D. R. Gray, Z. Li, R. Slavík, and D. J. Richardson, "Towards high-capacity fiber-optic communications at the speed of light in vacuum," Nat. Photonics **7**, 279–284 (2013).
5. P. J. Roberts, F. Couny, H. Sabert, B. J. Mangan, D. P. Williams, L. Farr, M. W. Mason, A. Tomlinson, T. A. Birks, J. C. Knight, and P. St. J. Russell, "Ultimate low loss of hollow-core photonic crystal fibers," Opt. Express **13**, 236–244 (2005).
6. A. D. Ellis, J. Zhao, and D. Cotter, "Approaching the non-linear Shannon limit," J. Lightwave Technol. **28**, 423–433 (2010).
7. S. Shibata, M. Horiguchi, K. Jinguji, S. Mitachi, T. Kanamori, and T. Manabe, "Prediction of loss minima in infra-red optical fibers," Electron. Lett. **17**, 775–777 (1981).
8. R. A. Garnham, D. G. Cunningham, and W. A. Stallard, "34 Mbit/s optical fiber transmission system experiment at a wavelength of 2.4 μm," Electron. Lett. **23**, 1063–1064 (1987).
9. R. Phelan, J. O'Carroll, D. Byrne, C. Herbert, J. Somers, and B. Kelly, "$In_{0.75}Ga_{0.25}As/InP$ multiple quantum-well discrete-mode laser diode emitting at 2 μm," IEEE Photon. Technol. Lett. **24**, 652–654 (2012).
10. J. Leuthold, C. Koos, and W. Freude, "Nonlinear silicon photonics," Nat. Photonics **4**, 535–544 (2010).
11. J. J. Ackert, D. J. Thomson, L. Shen, A. C. Peacock, P. E. Jessop, G. T. Reed, G. Z. Mashanovich, and A. P. Knights, "High-speed detection at two micrometres with monolithic silicon photodiodes," Nat. Photonics **9**, 393–396 (2015).
12. R. Wang, S. Sprengel, M. Muneeb, G. Boehm, R. Baets, M. C. Amann, and G. Roelkens, "2 μm wavelength range InP-based type-II quantum well photodiodes heterogeneously integrated on silicon photonic integrated circuits," Opt. Express **23**, 26834–26841 (2015).
13. E. J. Stanton, N. Volet, and J. E. Bowers, "Silicon arrayed waveguide gratings at 2.0-μm wavelength characterized with an on-chip resonator," Opt. Lett. **43**, 1135–1138 (2018).
14. N. Volet, A. Spott, E. J. Stanton, M. L. Davenport, L. Chang, J. D. Peters, T. C. Briles, I. Vurgaftman, J. R. Meyer, and J. E. Bowers,

"Semiconductor optical amplifiers at 2.0-μm wavelength on silicon," Laser Photon. Rev. **11**, 1600165 (2017).
15. M. S. Rouifed, C. G. Littlejohns, G. X. Tina, H. Qiu, J. S. Penades, M. Nedeljkovic, Z. Zhang, C. Liu, D. J. Thomson, G. Z. Mashanovich, G. T. Reed, and H. Wang, "Ultra-compact MMI-based beam splitter demultiplexer for the NIR/MIR wavelengths of 1.55 μm and 2 μm," Opt. Express **25**, 10893–10900 (2017).
16. H. Zhang, M. Gleeson, N. Ye, N. Pavarelli, X. Ouyang, J. Zhao, N. Kavanagh, C. Robert, H. Yang, P. E. Morrissey, K. Thomas, A. Gocalinska, Y. Chen, T. Bradley, J. P. Wooler, J. R. Hayes, E. Numkam Fokoua, Z. Li, S. U. Alam, F. Poletti, M. N. Petrovich, D. J. Richardson, B. Kelly, J. O'Carroll, R. Phelan, E. Pelucchi, P. O'Brien, F. Peters, B. Corbett, and F. Gunning, "Dense WDM transmission at 2 μm enabled by an arrayed waveguide grating," Opt. Lett. **40**, 3308–3311 (2015).
17. Z. Liu, Z. Li, Y. Chen, J. P. Wooler, B. Kelly, R. Phelan, J. O'Carroll, N. V. Wheeler, A. M. Heidt, F. Poletti, M. N. Petrovich, S. U. Alam, D. J. Richardson, and R. Slavík, "Up to 64QAM (30 Gbit/s) directly-modulated and directly detected OFDM at 2 μm wavelength," in *European Conference on Optical Communication (ECOC)* (2014), paper Tu.4.3.5.
18. F. Amzajerdian, D. Pierrottet, U. Singh, and M. Kavaya, "Optimum integrated heterodyne photoreceiver for coherent lidar applications," in *MRS Proceedings* (2005), Vol. **883**, paper FF6.3.
19. N. Ye, M. Gleeson, H. Yang, H. Zhang, B. Roycroft, K. Thomas, A. Gocalinska, E. Pelucchi, Z. Li, D. Richardson, H. Chen, A. M. J. Koonen, W. Jia, J. Zhao, F. Garcia Gunning, F. Peters, and B. Corbett, "Demonstration of 90° optical hybrid at 2 μm wavelength range based on 4 × 4 MMI using diluted waveguide," in *European Conference on Optical Communication (ECOC)* (2014), paper P. 2.14.
20. M. Lamy, C. Finot, J. Fatome, J. Arocas, J. C. Weeber, and K. Hammani, "10 Gbps data transmission in TiO_2 waveguides at 2 μm," Appl. Sci. **7**, 631 (2017).
21. M. Lamy, C. Finot, J. Fatome, M. Brun, P. Labeye, S. Nicolleti, A. Bogris, D. Syvridis, M. A. Ettabib, D. J. Richardson, P. Petropoulos, and K. Hammani, "Ten gigabit per second optical transmissions at 1.98 μm in centimetre-long SiGe waveguides," Electron. Lett. **53**, 1213–1214 (2017).
22. J. Li, Y. Liu, Y. Meng, K. Xu, J. Du, F. Wang, Z. He, and Q. Song, "2 μm wavelength grating coupler, bent waveguide, and tunable microring on silicon photonic MPW," IEEE Photon. Technol. Lett. **30**, 471–474 (2018).
23. N. Kavanagh, K. Shortiss, H. Zhang, M. Sadiq, K. Thomas, A. Gocalinska, Y. Zhao, E. Pelucchi, P. O'Brien, F. H. Peters, B. Corbett, and F. Gunning, "Impact of DWDM at 50 GHz spacing in the 2 μm waveband," in *Conference on Lasers and Electro-Optics (CLEO)* (2016), paper SF1F.5.
24. N. Mac Suibhne, Z. Li, B. Baeuerle, J. Zhao, J. P. Wooler, S. Alam, F. Poletti, M. N. Petrovich, A. Heidt, I. Giles, D. J. Giles, B. Pálsdóttir, L. Grüner-Nielsen, R. Phelan, J. O'Carroll, B. Kelly, D. Murphy, A. Ellis, D. Richardson, and F. C. Garcia Gunning, "Wavelength division multiplexing at 2 μm," in *European Conference on Optical Communication (ECOC)* (2012), paper Th.3.A.3.
25. W. Cotter, D. Goulding, B. Roycroft, J. O'Callaghan, B. Corbett, and F. H. Peters, "Investigation of active filter using injection-locked slotted Fabry–Perot semiconductor laser," Appl. Opt. **51**, 7357–7361 (2012).
26. Q. Béraud-Sudreau, J. B. Begueret, O. Mazouffre, M. Pignol, L. Baguena, C. Neveu, Y. Deval, and T. Taris, "SiGe clock and data recovery system based on injection-locked oscillator for 100 Gbit/s serial data link," IEEE J. Solid-State Circuits **49**, 1895–1904 (2014).
27. X. Jin and S. L. Chuang, "Bandwidth enhancement of Fabry–Perot quantum-well lasers by injection-locking," Solid-State Electron. **50**, 1141–1149 (2006).
28. E. K. Lau, L. J. Wong, and M. C. Wu, "Enhanced modulation characteristics of optical injection-locked lasers: a tutorial," IEEE J. Sel. Top. Quantum Electron. **15**, 618–633 (2009).
29. N. Kavanagh, B. Murray, D. Goulding, P. E. Morrissey, R. Sheehan, B. Corbett, and F. C. G. Gunning, "Enabling photonic technologies at 2 μm," in *International Conference on Transparent Optical Networks (ICTON)* (2017), paper Tu.B5.1.
30. H. Yang, N. Ye, R. Phelan, J. O'Carroll, B. Kelly, W. Han, X. Wang, N. Nudds, N. MacSuibhne, F. Gunning, P. O'Brien, F. H. Peters, and B. Corbett, "Butterfly packaged high-speed and low leakage InGaAs quantum well photodiode for 2000 nm wavelength systems," Electron. Lett. **49**, 281–282 (2013).
31. N. Ye, M. R. Gleeson, M. U. Sadiq, B. Roycroft, C. Robert, H. Yang, H. Zhang, P. E. Morrissey, N. Mac Suibhne, K. Thomas, A. Gocalinska, E. Pelucchi, R. Phelan, B. Kelly, J. O'Carroll, F. H. Peters, F. C. Garcia Gunning, and B. Corbett, "InP-based active and passive components for communication systems at 2 μm," J. Lightwave Technol. **33**, 971–975 (2015).
32. N. Ye, H. Yang, M. Gleeson, N. Pavarelli, H. Zhang, J. O'Callaghan, W. Han, N. Nudds, S. Collins, A. Gocalinska, E. Pelucchi, P. O'Brien, F. C. G. Gunning, F. H. Peters, and B. Corbett, "InGaAs surface normal photodiode for 2 μm optical communication systems," IEEE Photon. Technol. Lett. **27**, 1469–1472 (2015).
33. Z. Li, A. M. Heidt, J. M. O. Daniel, Y. Jung, S. U. Alam, and D. J. Richardson, "Thulium-doped fiber amplifier for optical communications at 2 μm," Opt. Express **21**, 9289–9297 (2013).
34. P. Kadwani, R. A. Sims, J. Chia, F. Altal, L. Shah, and M. C. Richardson, "Atmospheric gas detection using broadband mid-IR thulium fiber-based sources," Proc. SPIE **8039**, 80390L (2011).
35. E. Russell, N. Kavanagh, K. Shortiss, and F. C. G. Gunning, "Development of thulium-doped fiber amplifiers for the 2 μm waveband," Proc. SPIE **10683**, 10683Q (2018).
36. M. N. Petrovich, N. K. Baddela, N. V. Wheeler, E. Numkam, R. Slavík, D. R. Gray, J. R. Hayes, J. P. Wooler, F. Poletti, and D. J. Richardson, "Development of low loss, wide bandwidth hollow core photonic bandgap fibers," in *Optical Fiber Communications Conference and Exhibition (OFC)* (2013), paper OTh1J3.

143.239.102.147 {ts '2018-09-11 10:55:01'}